

# **Jointly spatial-temporal representation learning for individual trajectories**

Fei Huang <sup>a,b</sup>, Jianrong Lv <sup>a,b</sup> and Yang Yue <sup>a,b</sup> \*

<sup>a</sup> *Department of Urban Informatics, School of Architecture and Urban Planning, Shenzhen University, China*

<sup>b</sup> *Shenzhen Key Laboratory of Spatial Smart Sensing and Services, Shenzhen, China*

\* *Corresponding author, e-mail: yueyang@szu.edu.cn*

# Jointly spatial-temporal representation learning for individual trajectories

Individual trajectories, rich in human-environment interaction information across space and time, serve as vital inputs for geospatial foundation models (GeoFMs). However, existing attempts at learning trajectory representations have overlooked the implicit spatial-temporal dependency within trajectories, failing to encode such dependency in a deep learning-friendly format. That poses a challenge in obtaining general-purpose trajectory representations. Therefore, this paper proposes a spatial-temporal joint representation learning method (ST-GraphRL) to formalize learnable spatial-temporal dependencies into trajectory representations. The proposed ST-GraphRL consists of three compositions: (i) a weighted directed spatial-temporal graph to explicitly construct mobility interactions in both space and time dimensions; (ii) a two-stage jointly encoder (i.e., decoupling and fusion), to learn entangled spatial-temporal dependencies by independently decomposing and jointly aggregating space and time information; (iii) a decoder guides ST-GraphRL to learn explicit mobility regularities by simulating the spatial-temporal distributions of trajectories. Tested on three real-world human mobility datasets, the proposed ST-GraphRL outperformed all the baseline models in predicting movement spatial-temporal distributions and preserving trajectory similarity with high spatial-temporal correlations. Analyzing spatial-temporal features presented in latent space validates that ST-GraphRL understands spatial-temporal patterns. This study may also benefit representation learnings of other geospatial data to achieve general-purpose data representations and advance GeoFMs development.

Keywords: trajectory representation learning; spatial-temporal joint distribution; graph deep learning; spatial-temporal mobility patterns; foundation model for geospatial intelligence

## 1. Introduction

The emergence of foundation models like GPT, Llama, and DALL-E, which are trained on large amounts of data and can be tailored to a range of downstream tasks, has triggered a paradigm shift in artificial intelligence (AI). Representation learning is regarded as a crucial technique for foundation models because it offers a unified vector representation of information to effectively capture and comprehend a subject matter (Bengio et al., 2013;

Bommasani et al., 2022; Ericsson et al., 2022). Geospatial Foundation models, or GeoFMs, are also gaining increasing attention (Janowicz et al., 2020; Mai et al., 2023). Similarly, the effectiveness of GeoFMs is profoundly influenced by geospatial data representations (or features) that are implemented in learning geographical knowledge (Janowicz et al., 2020; Scheider & Richter, 2023). Most of the existing attempts, however, represent spatial and temporal information implicitly, resulting in the limited modelling capacity of GeoFMs (Zhang, et al., 2023).

Individual trajectory data—typical human active data indicating interactions between humans and the environment over space and time—is regarded as a fundamental aspect of the study on human-environment relations (Hägerstrand, 1970; Biljecki et al., 2013). Despite there being abundant coordinate points, travel points in trajectories are usually sparse and provide limited activity information (Gong et al., 2020). Furthermore, individual trajectories sampled with irregular frequency contain a significant variety of structures. This complexity makes it challenging to model continuous time variables and discrete location variables in trajectories to learn latent spatial-temporal dependencies. Sequential structure models such as LSTM (Hochreiter & Schmidhuber, 1997) and Transformer (Vaswani et al., 2017) have been used to capture mobility location regularities hidden in the continuous time dimension while ignoring the structure information between non-consecutive locations (Jiang et al., 2022). Structured graphs leveraging deep learning models like GNN (Veličković et al., 2018) have recently been employed to discover high-order correlation relations between trajectories. As each movement in trajectories represents a joint distribution over space and time, these approaches still require enhancement to explicitly and accurately capture the spatial-temporal dependency (Jiang et al., 2017; Schneider et al., 2013).

Therefore, this study proposes a joint spatial-temporal trajectory graph representation learning method (ST-GraphRL) to generate accurate and generalized trajectory representation via explicitly structured spatial-temporal information. The contributions of this work are two-fold:

- A novel directed spatial-temporal trajectory graph (ST-Graph) is constructed. The ST-Graph can explicitly present and extract the interdependent structural relations between locations and time concealed within sparse movements, overcoming structural design limitations in irregular trajectories with arbitrary lengths.

- A two-stage joint encoding framework is developed for individual trajectory representation (ST-GraphRL). This framework demonstrates proficiency in modelling spatial-temporal joint distributions and learning the intricate dependencies within trajectories, providing useful general-purpose representation for a wide range of downstream tasks on human mobility.

The remainder of this paper is organized as follows. Section 2 reviews previous work on representation learning for trajectory, and Section 3 future gives definitions. In Section 4, we introduce the proposed ST-GraphRL model and its technical details. Section 5 reports on data processing and experimental results. We take discussions in Section 6. In the final section, we provide insights on future work in addition to a summary.

## 2. Related work

Representation learning, the process of acquiring low-dimensional general-purpose features or representations of data, is crucial for AI to discern and disentangle underlying explanatory factors from low-level sensory data (Bengio et al., 2013). This part reviews representation learning primarily through the lens of deep learning algorithms which is the dominant approach to representation learning at the current stage. Deep learning achieves representation learning by composing multiple non-linear transformations, automatically yielding representations applicable to various downstream tasks, spanning recognition, classification, and prediction (Ericsson et al., 2022; Grill et al., 2020). It spans across diverse data modalities including images (Caron et al., 2020), text (Devlin et al., 2019), and graphs (Veličković, et al., 2018). As typical spatial-temporal data, trajectory consists of consecutive (from a sequence) or spatially nearby observations. Consequently, the purpose of trajectory representation learning is to transform and compress the spatial-temporal distribution of raw trajectories into generic low-dimensional representation vectors, empowering the downstream tasks such as trajectory similarity computation (Glake et al., 2022), traffic prediction (Zhang, et al., 2023), and urban structure analysis (Hu et al., 2023). In trajectory representation learning, a trajectory can take two forms: as a sequence or a structured graph (Barbosa et al., 2018), either way, both temporal and spatial features are two indispensable factors that should be embedded into the trajectory representation (Damiani et al., 2020).

To handle the consecutive temporal dimension, trajectories are usually fed into a model

as the ordered coordinates. Such as *t2vec* (Li et al., 2018) considered trajectories as sequences of GPS sample points and learned the representation by reconstructing high-sampling trajectory sequences from low-sampling sequences. However, the reconstruction process did not match the temporal information under the sequential time order. As to model the feature relation between time  $t$  and  $t+1$ , both LSTM-based and Transformer (Self-attention-based) models are feasible approaches that can capture the high-order correlations in mobilities. Although LSTM has been utilized to extract user mobility patterns from the check-in data (Gao et al., 2017; Kong & Wu, 2018), it is susceptible to disturbances caused by sparse and discontinuous data, which further complicates the identification of dependencies in movements (Glake et al., 2022). The Self-attention-based model enhances the ability to capture contextual features by dynamically allocating attention weights to different locations in the input trajectory over time; however, learning spatial transit relationships in moving processes remains challenging (Jiang et al., 2022; Fang et al., 2022). Furthermore, directly feeding a series of trajectories into either LSTMs or Self-attention-based models for temporal dimensional learning is ineffective, since it fails to address temporal characteristics adequately.

Since spatial linkages are identifiable through the graphical structure, graph deep learning has become a popular method for processing trajectory data (Martin et al., 2023; Tao et al., 2022). In this way, the trajectory is regarded as a structured graph in which the visited locations are represented as nodes and the mobilities are represented as edges. Such as user activity graphs (P. Wang et al., 2019; M. Li et al., 2021) and spatial knowledge graphs (Wang et al., 2021) have been constructed to quantify individuals' mobility characteristics. Generally, road networks possess the inherent advantage in describing spatial activity relationships, thus, road representations can be converted into trajectories through marked locations and then separately training sequence learning model with a self-supervised task to learn trajectory representations (Chen et al., 2021; Yang et al., 2021). However, this kind of method separated space or time dimension, treating space and time distribution, i.e.,  $p(s)$  and  $p(t)$ , as two completely independent variables, which overlooks the spatial-temporal interactions in trajectories. Therefore, researchers have attempted to integrate structural information with sequential information and extract their dependent relationships to learn coupled spatial-temporal features (Zhang et al., 2020; Gao et al., 2022; J. Liu et al., 2023; Yu & Wang, 2023). In which the

GNN usually be used for the spatial structures embedding by capturing the long-range correlation between travels, then a sequential-structure model such as LSTM network or Self-attention-based model following to independently model temporal correlations in trajectories. However, these methods are to decompose the spatial-temporal distribution into conditionally dependent distributions, i.e.,  $p(t)$  and  $p(s|t)$ , in which spatial relationships are presented explicitly, while temporal information as an implicit condition in calculation. That may lead to restricted learning of spatial-temporal correlations. Additionally, the existing work based on spatial-temporal graph, such as integrated space and time dimensions of mobility data into node features (Liu et al., 2022), is hindered by complex and ambiguous spatial-temporal relationships in movements.

A review of prior research reveals a research gap regarding the joint representation of space and time, particularly given the difficulty of explicitly representing the temporal dimension. Thus, this study developed the ST-Graph to encode both spatial and temporal aspects while learning the joint spatial-temporal distribution of trajectories.

### 3. Preliminaries

#### 3.1 Definitions

**Definition 3.1.1 Individual Mobility Graph.** Given a trajectory sequence set  $\mathcal{R}(u) = (\mathcal{S}_1, \mathcal{S}_2, \dots, \mathcal{S}_{\mathcal{T}})$  of user  $u \in U$ , in which  $\mathcal{S}_{\mathcal{T}} = (l_1, \dots, l_i)$  is the trajectory in the  $\mathcal{T}$ -th day, and  $l_i \in |\mathcal{S}_{\mathcal{T}}|$  is the  $i$ -th location user visited. Individuals' trajectories are reconstructed as a graph  $\mathcal{G} = (\mathcal{V}, \mathcal{E}, \mathcal{W})$ , where  $\mathcal{V} = \langle \omega_j^{1 \times C_s} \rangle_{j=1}^{|\mathcal{V}|}$  is the vertexes set, and  $\mathcal{E} = \langle e_j^{1 \times C_t} \rangle_{j=1}^{|\mathcal{V}|-1}$  is the edge set;  $C_s$  and  $C_t$  refer to the length of vectors in  $\mathcal{V}$  and  $\mathcal{E}$ , respectively. Detailly, vertexes are locations information (i.e., POI categories), edges are transit vectors about time, and the edges' weight consists of transit frequency, distance, and duration between two locations. The entire structure preserves the relationships between vertexes and edges and can reflect individuals the general preferences patterns over space and time scales.

**Definition 3.1.2. Mobility Distribution.** There,  $P(\Phi_s|\mathcal{V})$ ,  $P(\Phi_t|\mathcal{E})$ , and  $P(\Phi_{t,s}|\mathcal{H})$ ,  $\mathcal{H}$  is the latent representation of  $\mathcal{G}$ .  $\Phi_s \in \mathbb{R}^{U \times C_s}$ ,  $\Phi_t \in \mathbb{R}^{U \times C_t}$ , and  $\Phi_{t,s} \in \mathbb{R}^{U \times C_s \times C_t}$  denote the matrix of POI categories distributions, travel timing distributions, and spatial-temporal distributions of trajectories in  $u$ , respectively.

### 3.2 Problem statement

This paper investigates the problem of learning mobility representation from individual trajectories by spatial-temporal graph. Formally, given a set of mobility graphs, we aim to find a mapping function  $f: \mathcal{G} \rightarrow \mathcal{H}$ , where  $\mathcal{H}$  is the vectorized representation of trajectories for an individual, being subject to the constraints of the mobility distribution.

## 4. Method

The proposed method, as shown in Figure 1, consists of three essential parts: (i) constructing an individual mobility graph to represent an individual’s mobility pattern; (ii) developing a GNN-based representation learning framework to learn low-dimensional vectorial representation from an individual’s trajectory graph; and (iii) evaluating the learned representation by imitating the distribution of trajectories.

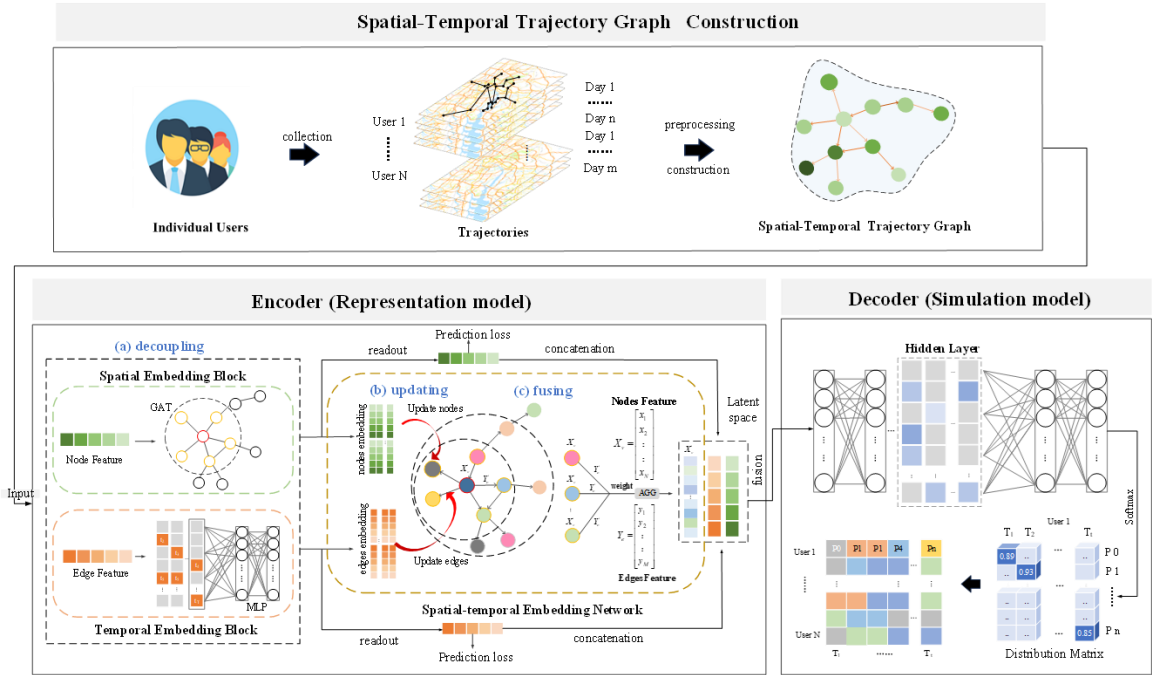


**Figure 1.** Workflow of ST-GraphRL.

### 4.1 Spatial-temporal trajectory graph

This section introduces how to construct a directed spatial-temporal trajectory graph  $\mathcal{G}$  to organize sparse trajectory data. The conventional approaches construct graphs by combining the spatial-related information such as locations and POI categories, with time information to form node features, which overlooks features in mobility transfers and breaks spatial-temporal interactions in movements. Thus, we regard the temporal

variation as a transition between trajectory points and design a transit vector of time between two nodes, which is denoted as an edge attribution. Meanwhile, the statistics descriptions (i.e., frequency, duration, and distance) are calculated as the weight for edges.

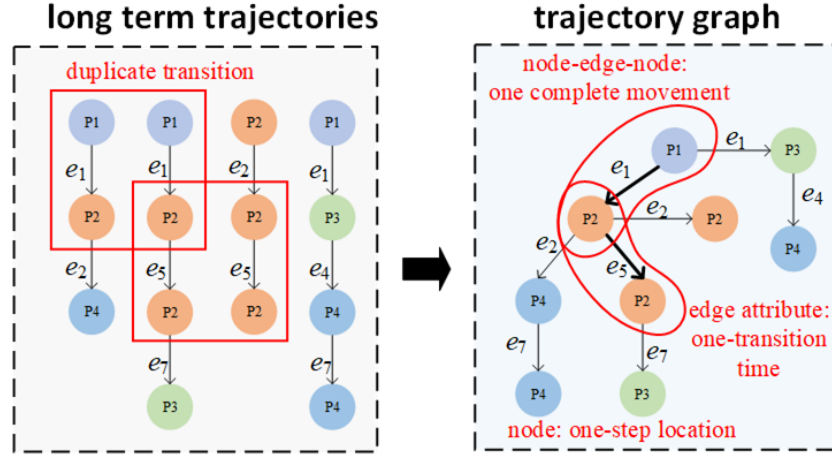


**Figure 2.** Details of the construction to the spatial-temporal trajectory graph of individual. one complete movement, presented in the form of node-edge-node, includes origin-destination and start-end time; for example, the user left from place P1 at 8:30 am and arrived at place P2 at 10:00 am, where  $e_i$  indicates its transit time i.e., from 8:30am to 10:00am. duplicate transition refers to two or more identical complete movements, and its identified mobility frequency is visually reflected by the thickness of the edge.

As the example shown in the Figure 2, lengths of trajectories collected in the long term are not consistent and the information in a trajectory is sparse, up to four movement points.  $\mathcal{G}$  builds the mobility regularity and randomness across multiple trajectories by utilizing these transit attributes (i.e.,  $e_i$  and duplicate transition) as the linking bridge. In this example, since the individual is more likely to move from P1 to P2 than to P3 in time-period  $e_1$ , as well as preferring moving from P2 to P2 in time-period  $e_5$  than in  $e_2$ . (see the red rectangles in the trajectory graph). Therefore,  $\mathcal{G}$  denotes  $P1-e_1-P2$  and  $P2-e_5-P2$  with a higher wight (marked by the red circles) than  $P1-e_1-P3$  and  $P2-e_2-P2$ , which captures the temporal and spatial routines in travel transitions, meanwhile preserving randomness in movements. It is found that  $\mathcal{G}$  describes a travel as an explicit transition in both time and location, where time acts as a mediator between shifting location information, such that explicitly building the intricate spatial-temporal interaction from irregular trajectories with sparse information

#### 4.2 Representation module

To effectively represent the coupling correlations between space and time in trajectories, we designed a two-stage encoder. It models the entangled space and time



features by decomposing the learning into two steps: decoupling and fusing. As shown in Figure 1 (a), the encoder independently learns decoupled spatial distribution and temporal distribution, i.e.,  $p(s)$  and  $p(t)$ , by the spatial embedding block and temporal embedding block, respectively. Then, graph  $\mathcal{G}$  is updated by the embeddings decoupled in (a), and then fusing them to capture low-dimensional spatial-temporal dependencies, i.e.,  $p(s_{i+1}|s_i, t_i)$  and  $p(t_{i+1}|s_i, t_i)$  by the message passing and aggregation operation of the spatial-temporal network, as shown in Figure 1.

#### 4.2.1 Decoupling spatial-temporal information

$\mathcal{V}$  and  $\mathcal{E}$  refer to space information and time information decoupled from  $\mathcal{G}$ , respectively, in which  $\mathcal{V}$  and  $\mathcal{E}$  are fully independent. Spatial embedding block works based on a GAT model (Veličković et al., 2018), which helps to learn the topology of locations in mobility trajectory, hence  $\hat{\mathcal{V}} = f_{GAT}(\mathcal{V})$ . Temporal embedding block relies on a stack of multilayer perceptron (MLP) units, in which  $\hat{\mathcal{E}} = f_{MLP}(\mathcal{E})$ . Furtherly, distributions  $P(\Phi_s|\mathcal{V})$  and  $P(\Phi_t|\mathcal{E})$  are regarded as the guidance of training for  $\hat{\mathcal{V}}$  and  $\hat{\mathcal{E}}$ , such that the preliminary embeddings containing completely latent regularities in space and time can be achieved. Here,  $\Phi_s = f_{sq-s}(\text{meanpool}(\hat{\mathcal{V}}))$ , and  $\Phi_t = f_{sq-t}(\text{sum}(w_t * \hat{\mathcal{E}}))$ ,  $w_t$  denotes a trainable weight for time information,  $f_{sq-s}$  and  $f_{sq-t}$  refer to the linear mapping for spatial embeddings and temporal embeddings.

#### 4.2.2 Learning spatial-temporal dependency

Learning spatial-temporal jointly embedding for mobility trajectories, which involves estimating the probability distribution  $p(s, t)$  linked to time  $t$  and location  $s$ , is intractable but crucial for capturing spatial-temporal patterns of movements. However, most previous researches have modeled it under the assumption of conditional independence. For example, the general approach extracts the temporal distribution  $p(t)$ , and then the conditional distribution  $p(s|t)$  for spatial information. The information derived from the representation learned through  $p(s|t)$  is implicit and constrained, revealing reduced expressiveness. Thus, we design jointly encoding to fuse the well-embedded space and time features in section 4.2.1, and learn spatial-temporal dependencies. In this part,  $\mathcal{G}$  is updated to  $\hat{\mathcal{G}} = (\hat{\mathcal{V}}, \hat{\mathcal{E}}, \mathcal{W})$ , then a generalized GNN model (Li et al., 2020) with three layers is employed to capture the interdependence in spatial and temporal domains, which facilitates the next learning of spatial-temporal joint distributions. Detailly, the message updating of vertex  $\mathcal{v}$  is shown as:

$$m_{vu}^l = \rho^l(h_v^l, h_u^l, h_{e_{vu}}^l) = \text{ReLu}(h_u^l + h_{e_{vu}}^l + h_{w_{vu}}^l) + \epsilon \quad (1)$$

$$m_{e_{vu}}^l = \text{MLP}\left(\text{Concate}(h_v^l, h_u^l)\right) \quad (2)$$

where  $\zeta^l(\cdot)$  is the message aggregation function which outputs the aggregated message  $m_v^l$ ;  $h_v^l$  is the vertex features in the  $l$ -th layer, its neighbor's features  $h_u^l$ , the feature of edge attribute  $h_{e_{vu}}^l$ , and the normalized edge weight  $h_{w_{vu}}^l$ . There are two different aggregation operations for nodes and edges, written as:

$$\zeta_v^l = \sum_{u \in \hat{\mathcal{V}}} \frac{\exp(\beta m_{vu})}{\sum_{i \in \mathcal{N}(\hat{\mathcal{V}})} \exp(\beta m_{vi})} \quad (3)$$

$$m_v^l = \zeta_v^l(\{m_{vu}^l | u \in \hat{\mathcal{V}}\}) \quad (4)$$

$$h_v^{l+1} = \phi^l(h_v^l, m_v^l) = \text{MLP}\left(h_v^l + s \cdot \frac{\|h_v^l\|_2}{\|m_v^l\|_2} \cdot m_v^l\right) \quad (5)$$

$$h_{e_{vu}}^{l+1} = \phi^l(h_{e_{vu}}^l, m_{e_{vu}}^l) \quad (6)$$

As described above, the process of message passing, every updating for vertex and corresponding edge, seen as the joint estimation in  $f(\hat{\mathcal{V}}^{l+1} | \hat{\mathcal{V}}^l, \hat{\mathcal{E}}^l)$  and  $f(\hat{\mathcal{E}}^{l+1} | \hat{\mathcal{V}}^l, \hat{\mathcal{E}}^l)$ , is the learning of interactive information in space and time, such that generating the final representation  $\mathcal{H}$  of the user.

$$a_w = \text{softmax}(\text{MLP}(h_w)), a_w \in \mathbb{R}^{(|\hat{\mathcal{V}}|-1) \times 1} \quad (7)$$

$$m_{\hat{\mathcal{V}}} = \text{MLP}\left(\text{concat}(h_v, h_{e_{vu}}, h_u)\right), (v, u) \in \hat{\mathcal{V}} \quad (8)$$

$$\mathcal{H} = \text{sum}(a_w \cdot m_{\hat{\mathcal{V}}}), \mathcal{H} \in \mathbb{R}^{1 \times d} \quad (9)$$

where  $d$  refers to the numbers of dimensions in  $\mathcal{H}$ , it is set  $d = 24$ .

### 4.3 Simulation module

To ensure the latent state  $\mathcal{H}$  captures the pattern of spatial-temporal transition in long-term movements, we designed a simulation stage that can be regarded as a decoder to reconstruct the spatial-temporal distribution from  $\mathcal{H}$ . If the reconstruction is well accomplished, entangled spatial-temporal patterns can be learned for representation. The input of the simulation module is  $z = (\mathcal{H}, \Phi_s, \Phi_t)$ . As shown in Figure 1, several dense MLP units, here we stacked three units with residual structure, are utilized to explore the most possible location and time for individual's movements.

$$\Phi_{t,s} = \mathcal{F}_{MPL}(z) \quad (10)$$

### 4.4 Loss function

We treat the training as the multi-label recognition problems, thus guiding ST-

GraphRL to learn the accurate spatial-temporal distribution of mobility. The loss function includes: (i) Time distribution loss (in section 4.2.1) and (ii) Space distribution loss (in section 4.2.1), which aims to minimize the modeling error in capturing travel time/place preferences by simulating the distribution of time occurrences/visited places, guiding the model to learn temporal/spatial information embedded in user trajectories; and (iii) similarly, time-space joint distribution loss is designed to learn the spatial-temporal dependency (in section 4.2.2). Note that we employ the distribution balance loss(Wu et al., 2021) to overcome the bias of travel time and visited places for individual trajectories and minimize the overall loss  $L$  as follows, where  $\hat{r}_i^k$  is a re-balancing weight,  $z_i^k$  denotes the variation of  $x^k$ ,  $x_s = \text{sigmoid}(\Phi_s)$ ,  $x_t = \text{sigmoid}(\Phi_t)$ , and  $x_{st} = \text{softmax}(\Phi_{t,s})$

$$L_{DB}(x^k, y^k) = \frac{1}{C} \sum_{i=0}^C \hat{r}_i^k [y_i^k \log(1 + e^{-(z_i^k - v_i)}) + \frac{1}{\lambda} (1 - y_i^k) \log(1 + e^{-(z_i^k - v_i)})] \quad (11)$$

$$L = 0.1 * L_{DB}(x_s, y_s) + 0.1 * L_{DB}(x_t, y_t) + L_{DB}(x_{st}, y_{st}) \quad (12)$$

## 5. Experiments

### 5.1 Experimental Setup

#### 5.1.1 Datasets and preprocessing

We performed a series of comparison and ablation experiments on three real-world datasets obtained from open sources: (1) code scanning data in Chengdu, located in Sichuan Province, China, for a month; (2) Check-in dataset in Tokyo, Japan; and (3) Check-in dataset in New York, USA. Dataset (1) is associated with timestamps and GPS coordinates, while datasets (2) and (3) (Yang et al., 2015) have extra information about POI category of the check-in place.

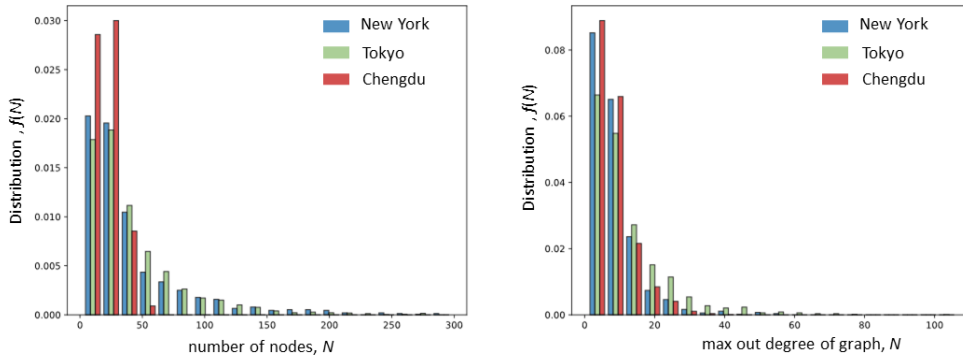


**Figure 3.** Statistics of the trajectory graphs.

**Table 1.** Statistics of the experimental data.

City	Sequences	Graphs	Edges	POI category	Time Period
Chengdu	1,453,219	113,109	2,319,243	-	2021.11.01- 2021.11.30
New York	227,428	1,041	46,503	251	2012.04.12- 2013.02.16
Tokyo	573,703	2,223	93,119	247	

Before implementing the proposed ST-GraphRL, we need to reprocess these check-in datasets to construct STJ-Graph to capture and organize original spatial-temporal information as the data input. First, to capture the regularity in the individual trajectories, we excluded the individuals with less than three trajectories while ensuring that there are at least two check-in points in the retained trajectories, i.e., at least one complete mobility transition. The distance, time spent, and frequency of movement were calculated as the weights of movements. Considering the sparsity of the check-in data and the computational overhead, we divide the time interval in the trajectory into 30 minutes, which can be represented through a 48-dimensional vector with start-end time to describe the transitive information of the movement over time. The category of POIs in datasets (2) and (3) are 251 and 247, respectively, and we summarized them into 10 classes including residential areas, education, food places, transportation, medical, offices/workplaces, personal services, government offices, outdoor and recreation places, and others. Since there is no POIs information in dataset (1), we constructed a simple origin-destination network, where the node features consisted of the land use information and the flow of people, to learn features for each check-in location; we employed Gaussian Mixture model to cluster these features, thus achieving the semantic category for the code scanning place, and the optimal number of clusters were 8 classes.

Table 1 shows the statistical information of datasets, and Figure 3 presents that the number of nodes and the maximum outdegree of each graph confirm the power-law distribution.

### 5.1.2 baseline models

To evaluate the performance of our proposed model, we designed ablation experiments and compare these models with other baseline models.

(1) **Summary trajectory.** The summary trajectory (Damiani et al., 2019) characterizes relevant locations and related mobility patterns in symbolic trajectories, here, symbolic locations are vectorized by word2Vec, and in the experiment  $N = 3$ ,  $\delta = 2\Delta$ .

(2) **Deep Graph Infomax, DGI.** DGI (Veličković et al., 2018) learns node

representations in an unsupervised manner by maximizing mutual information between patch representations and corresponding high-level summaries of graphs. We set the number of layers as 3 in the GNN model.

(4) **Self-attention-based network.** Self-attention (Vaswani et al., 2017) captures context by considering the importance of all elements in the sequence simultaneously, which can model longer-range dependencies effectively than LSTM. We set the hidden layer number as 4 with 8 multi-heads and the hidden channel is 64.

(5) Ablation model **ST-GraphRL-CST.** ST-GraphRL-CST removes the decoupling process from ST-GraphRL, which means that there is no spatial embedding block and temporal embedding block in ST-GraphRL-CST.

(6) Ablation model **ST-GraphRL-NTT.** ST-GraphRL-NTT moves the temporal information into the node feature, meaning that it cuts off the edge attribute.

(7) Ablation model **ST-GraphRL-DGI.** ST-GraphRL-DGI replaces the decoupling process used in ST-GraphRL with the linking prediction employed in DGI, such that comparing which kind of initial embedding over space and time is better to learn the coupled spatial-temporal dependency.

In summary, the Summary trajectory is a non-deep learning method specifically designed for trajectory representation considering location information; the Self-attention-based model performs well in extracting series relationships, and DGI enables capturing spatial relationships between movements. To ensure the equality of experiments, the decoder designed in ST-GraphRL was also added to baseline models for training. The Chengdu dataset was divided into two sets: 80% of the graphs were the training set and the remaining 20% graphs were the testing set. Since the sizes of the New York dataset and Tokyo dataset are small, we did not split the training set. All the evaluations were performed on a  $\times 64$  machine with a single GPU (NVIDIA RTX 1080Ti).

### 5.1.3 Evaluation Metrics

We evaluated the model performances on four metrics. Firstly, Accuracy, Precision, and F1 were utilized to evaluate the prediction for users' spatial-temporal distribution preference. Specifically, given the recorded data of user  $u_i$  to learn the representation  $z_i$ , and then utilizing  $z_i$  to jointly infer time periods in a certain day during which a movement is likely to occur and the category of location the user visited in that time. Additionally, suppose there exists a correlation between the mobility pattern and the distribution of the visit frequency, including time and place, coefficient  $r$  (Damiani et al.,

2020) was employed to reflect the goodness on the spatial-temporal correlation of embeddings.

**Table 2.** Evaluation of the prediction task.

Method	Datasets	Accuracy	Precision	F1
Summary Trajectory	New York	0.2983	0.1978	0.2320
	Tokyo	0.3075	0.2818	0.1670
	Chengdu	0.2656	0.3465	0.2016
DGI	New York	0.4337	0.4117	0.3954
	Tokyo	0.4947	0.4569	0.4616
	Chengdu	0.5076	0.4765	0.4402
Self-attention	New York	0.5406	0.5274	0.5192
	Tokyo	0.5772	0.5272	0.5104
	Chengdu	0.6716	0.5603	0.5684
ST-GraphRL-NTT	New York	0.5735	0.5562	0.5460
	Tokyo	0.5959	0.5530	0.5640
	Chengdu	0.6527	0.5541	0.5537
ST-GraphRL-CST	New York	0.5335	0.4915	0.5130
	Tokyo	0.5780	0.5135	0.5210
	Chengdu	0.6787	0.5615	0.5334
ST-GraphRL-DGI	New York	0.5602	0.5418	0.5225
	Tokyo	0.6081	0.6035	0.5560
	Chengdu	0.6750	0.5653	0.5470
ST-GraphRL	New York	0.7064	0.6302	0.6052
	Tokyo	0.7739	<b>0.6771</b>	<b>0.6548</b>
	Chengdu	<b>0.8540</b>	0.6451	0.6311

## 5.2 Experimental results and analysis

### 5.2.1 Comparison of prediction results

We compared our method with the baseline methods in the task of imitating the spatial-temporal distribution of individual trajectories in one day. The evaluation metrics including Accuracy, Precision, F1, and coefficient  $r$  are listed in Table 2. As shown in Table 2 that the Summary trajectory presents the lowest scores in all metrics, which may be because it cannot interpret trajectory similarity in terms of location similarity, moreover, its sequential structure is hard to deal with the temporal dimension of sparse trajectories. DGI outperformed the Summary trajectory with increased average score (  $\Delta accuracy: +0.19$ ,  $\Delta precision: +0.17$ ,  $\Delta F1: +0.23$  ) in three datasets, which demonstrates that the presentation of node-linking-node in the graph is effective to

represent movements; however, F1 scores achieved by DGI on three datasets are still less than 0.5, which indicates that DGI failed to capture movement patterns. The Self-attention achieved higher scores than DGI ( $\Delta accuracy: +0.12$ ,  $\Delta precision: +0.09$ ,  $\Delta F1: +0.10$ ), but its average F1 score is only 0.03 higher than 0.5. It indicates that although the Self-attention enables one to learn contexts from sparse features, it only captures partial, in certain time periods, mobility patterns. Our proposed method, ST-GraphRL, as expected, achieved the best performance with more than 0.6 scores in accuracy, precision, and F1 over both three datasets, demonstrating the effectiveness of joint spatial-temporal representation.

F1 scores of three ablation models, ST-GraphRL-CST, ST-GraphRL-NTT, and ST-GraphRL-DGI, fluctuated between 0.50-0.56, demonstrating the necessity of the components in ST-GraphRL. Detailly, compared to ST-GraphRL-NTT which discards the presentation specializing in temporal information, removing the step of decoupling result in a 0.2 decrease in F1 scores to ST-GraphRL-CST, suggesting that decoupling plays a vital role in clearing up entangled spatial-temporal relationships. The Self-attention performed comparably to ST-GraphRL-NTT on the Chengdu dataset, but scored lower than ST-GraphRL-NTT on the other two datasets, implying that larger datasets may improve Self-attention performance but that its sequential structure still confounds spatial-temporal dependence when temporal transitions between locations are not explicitly presented. When we retain the edge attribute used in ST-GraphRL, while replacing the decoupling strategy with linking prediction used in DGI, the ST-GraphRL-DGI achieved similar scores to that of ST-GraphRL-NTT, with improved performance compared with DGI. In summary, the results prove that joint encoding is the basis for accurately learning complex spatial-temporal dependencies in the moving process, which presupposes that the transfer relation in trajectories over space and time is explicitly constructed and that the decoupling-fusion strategy is an effective method for achieving efficient spatial-temporal joint modeling.

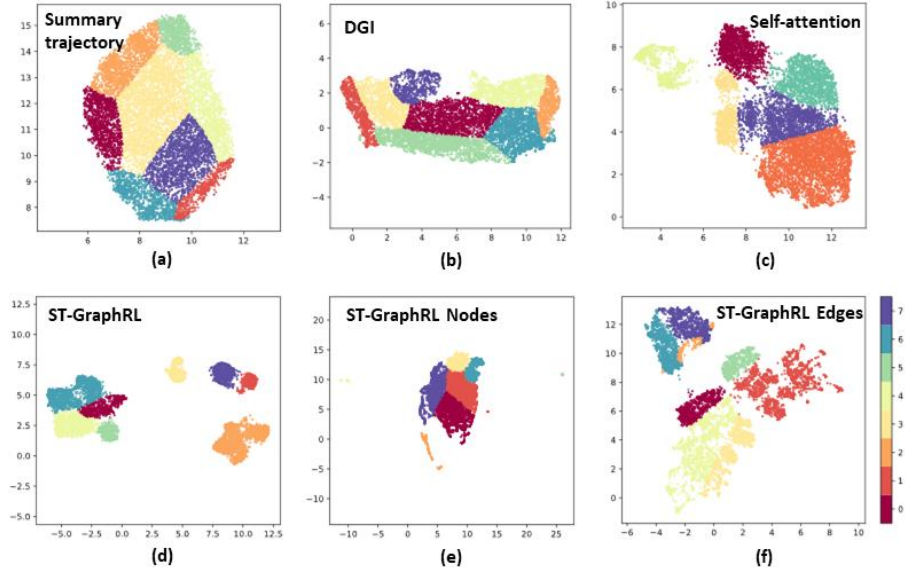


**Figure 4.** Dimensional reduction of trajectory representations with 8 clusters; Nodes refer to the vertex features of ST-GraphRL; Edges refer to the combination of one edge feature and two vertex features connected by the edge.

### 5.2.2 Visualization of embeddings

To further validate that ST-GraphRL can distinguish trajectory similarities, we reduced and visualized the representation space to 2-dimensions by UMAP. In Figure 4, the colored points are the clustered individuals. The spaces among each cluster in ST-GraphRL (Figure 4(d)), are much larger, such that clusters can easily be separated visually even without the color reference, which it failed to achieve in the Summary trajectory (Figure 4(a)), DGI (Figure 4(b)), and Self-attention (Figure 4(c)). Furthermore, we visualize the embedding of nodes and edges (node pairs) in ST-GraphRL (Figure 4(e-f)). It is found that edges present a comparable performance with the Self-attention, their embeddings are not particularly tightly clustered in single clusters, but there is comparably distinguishability between different clusters. It indicates that the features and patterns they captured may also be similar. Although there is compacted node embedding, ST-GraphRL shows better separability of its inter-cluster than that of edges and the Self-attention. It confirms that features learned in nodes and edges are different, focusing on independent patterns in the latent feature space, while fusing the two kinds of features helps to completely represent a movement. In contrast, the Self-attention can only capture partial features, i.e., the similarity between different trajectories rather than mobility patterns, as it cannot learn the interactive relationships over space and time hidden in trajectories. In summary, representations generated by the proposed ST-GraphRL can exactly measure the differences and similarities in individual trajectories, which is



attributed to the accurate representation of both spatial and temporal dimensions by its nodes and edges, as well as the modeling of the relationships between nodes and edges.

### 5.2.3 Visualization of trajectory graph

We visualized the trajectory graph for some randomized individuals to evaluate the distance among the respective representations. As seen in Figure 5, the color of nodes indicates POI's category, the arrow refers to the order of visits, and the thickness of the line represents the frequency of visits; in which graphs of individuals in different clusters show differences in the following aspects: the number of nodes, the category of nodes and node pairs, and the frequency of visits. As marked with red arrows in user 11134 and user 1105, they show similar movement sequences and visited frequency between two nodes, thus they are close in the clustering space. Also, the diversity, in terms of space and time, of trajectories can be reflected on the trajectory graph. Such as, user 10550 shows great regularity with fixed types and high frequencies of places to visit, while the movements of user 10005 are more random in temporal dimension as there are more node pairs with the same color. Although user 11024 and user 10550 have similar visited locations, the order of their visits is very different, e.g., user 11024 takes the path "yellow point  $\rightarrow$  yellow point  $\rightarrow$  pink point", while user 10550 takes the path "pink point  $\rightarrow$  pink point  $\rightarrow$  yellow point", thus they are not in the same cluster.

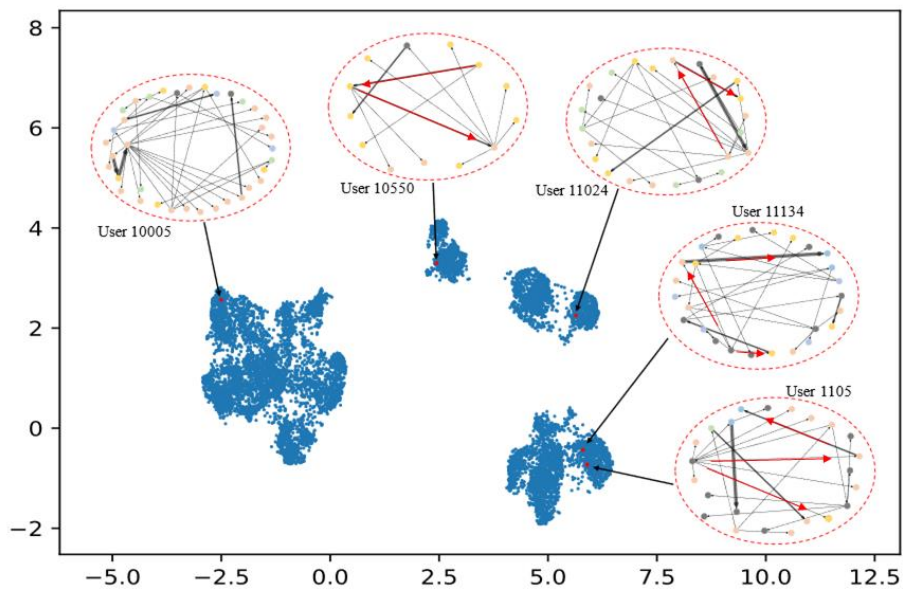


**Figure 5.** Trajectory graphs corresponding to embeddings represented by ST-GraphRL.

### 5.2.2 Validation of spatial-temporal dependency in representations

To further validate whether ST-GraphRL enables the capture of spatial-temporal dependency in trajectories, we employed the following approach: assuming that there is a specific spatial-temporal mobility pattern in each individual’s trajectories, and thus the similarity of mobility patterns between different individuals can be measured by calculating the distance ( $d_{true}$ ) of the movement spatio-temporal distribution matrix. If the distance between the trajectory representations ( $d_{rep}$ ) of individuals has a positive correlation ( $r$ ) with  $d_{true}$ , it suggests that the learned representation already encompasses the spatial-temporal dependency in trajectories and is representative of the individual mobility pattern. The Euclidean distance and the Jensen distance are utilized to calculate for  $d_{rep}$  and  $d_{true}$ . We measured the similarity of individual trajectories from three indicators, i.e., the distribution of categories of visited locations, the distribution of times when the movement occurred, and the spatial-temporal distribution of the movement, denoted by  $r_s$ ,  $r_t$ , and  $r_{st}$ , respectively.

As displayed in Table 3 and Figure 6, the representation of ST-GraphRL exhibits a strong coherence with the spatial-temporal distribution of trajectories, particularly on the Chengdu dataset with a coefficient  $r_{st}$  0.77. It confirms the existence of abstracted spatial-temporal dependency features in the latent space of ST-GraphRL representations. In contrast, the Summary Trajectory and DGI fail to capture spatial-temporal distribution, showing a negligible correlation  $r_{st}$  0.03 and very weak correlation  $r_{st}$  0.26 between their representation and the actual trajectory distribution, respectively, leading to their low scores reported in Table 2. The Self-attention excels at extracting relations between consecutive contexts, providing robust support for it to learn trajectories’ temporal distribution  $r_t$  0.56. However, the Self-attention ignores the features in movement transitions, resulting in decreased scores  $\Delta r_s = -0.17$  and  $\Delta r_{st} = -0.19$  compared to ST-GraphRL in the Chengdu dataset. The embeddings of nodes and edges in ST-GraphRL exhibit correlations with the distribution of trajectories in space and time, respectively. The node achieves the highest  $r_s$  0.55, the edge has the second highest  $r_t$  0.44 and  $r_{st}$  0.55, indicating that the node and edge in ST-GraphRL effectively represent the spatial and temporal features, respectively. Thus, integrating features from both nodes and edges enables ST-GraphRL to ultimately achieve the highest correlation  $r_t$  0.65 and  $r_{st}$  0.77. This validates that explicit structuring and decoupling of space and time (i.e., the edge and node) helps the extraction of accurate spatial and temporal features from

entangled information; and the jointly features fusing empowers ST-GraphRL in effectively learning spatial-temporal dependencies and distributions.

**Table 3.** Evaluation of the spatial-temporal dependency in embeddings in Chengdu, Tokyo, and New York dataset (CD, TKY, and NYK);  $r_s$ ,  $r_t$ , and  $r_{st}$ , respectively refers to the correlation with the distribution of location frequency, visited time-period frequency, and spatial-temporal frequency in trajectories. the higher the value of  $r$ , the better the performance of the model.

Method	$r_s$	$r_t$	$r_{st}$
	CD/ TKY/ NYK	CD/ TKY/ NYK	CD/ TKY/ NYK
ST-GraphRL	0.48/0.35/0.04	<b>0.65</b> /0.16/0.15	<b>0.77</b> /0.48/0.18
ST-GraphRL (Nodes)	<b>0.55</b> /0.55/0.02	0.00/0.17/0.06	0.29/0.39/0.16
ST-GraphRL (Edges)	0.32/0.18/0.09	0.44/0.28/0.11	0.55/0.40/0.38
DGI	0.24/0.16/0.04	0.33/0.12/0.06	0.26/0.12/0.02
Summary trajectory	0.05/0.03/0.01	0.03/0.06/0.01	0.03/0.00/0.03
Self-attention	0.31/0.12/0.04	0.56/0.16/0.12	0.58/0.31/0.12

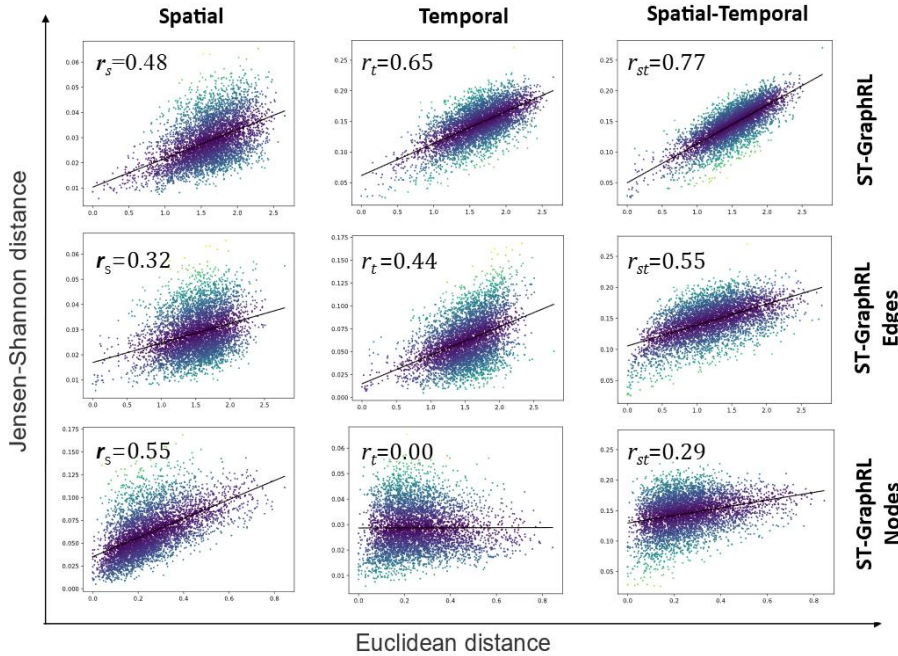


**Figure 6.** Scatter plot of points representing pairs of ST-GraphRL in the Sichuan dataset: the x-axis reports Euclidean distance of embedding pairs, the y-axis refers to Jensen distance of distributions of real trajectory pairs.

## 6. Discussions: neural responses to spatial-temporal patterns in latent space

The above results have demonstrated the ability of ST-GraphRL in representing space and time features. But how can the ST-GraphRL capture/express spatial-temporal interactions/patterns in trajectories? To answer the question, we further explore how the activated representation in latent space responds to spatial-temporal patterns that are described by two specific designed spatial-temporal indexes,  $I_{st}^1$  and  $I_{st}^2$ . Noting that, an effective response is defined as the observable and regular variation (e.g., a linear variation) of response strength to respond the changes of indexes:

$$I_{st}^1 = \sqrt{n_t^2 + n_s^2} \quad (13)$$

where  $n_t$  refers to the average daily number of movements, while  $n_s$  refers to the average number of different categories of places the user visits, here  $n_t$  and  $n_s$  are normalized. The higher  $I_{st}^1$ , the greater spatial-temporal diversity of an individual's mobility.

$$I_{st}^2 = \log \left( \frac{\sum_N^i d_i}{N} \right) \quad (14)$$

where  $d_i$  refers to the cosine similarity between the  $i$ -th movement and other  $N-i$  movements,  $N$  is the total number of moves made by an individual. Here,  $I_{st}^2$  is employed to evaluate the stability of mobilities over space and time. The higher the  $I_{st}^2$ , the greater the possibility of fluctuations in a regular mobility pattern, e.g., assuming the individual moves many times, there may be the same departure-arrival location, but the start-end time is different; or there is the same start-end time, but the departure or arrival locations are different.

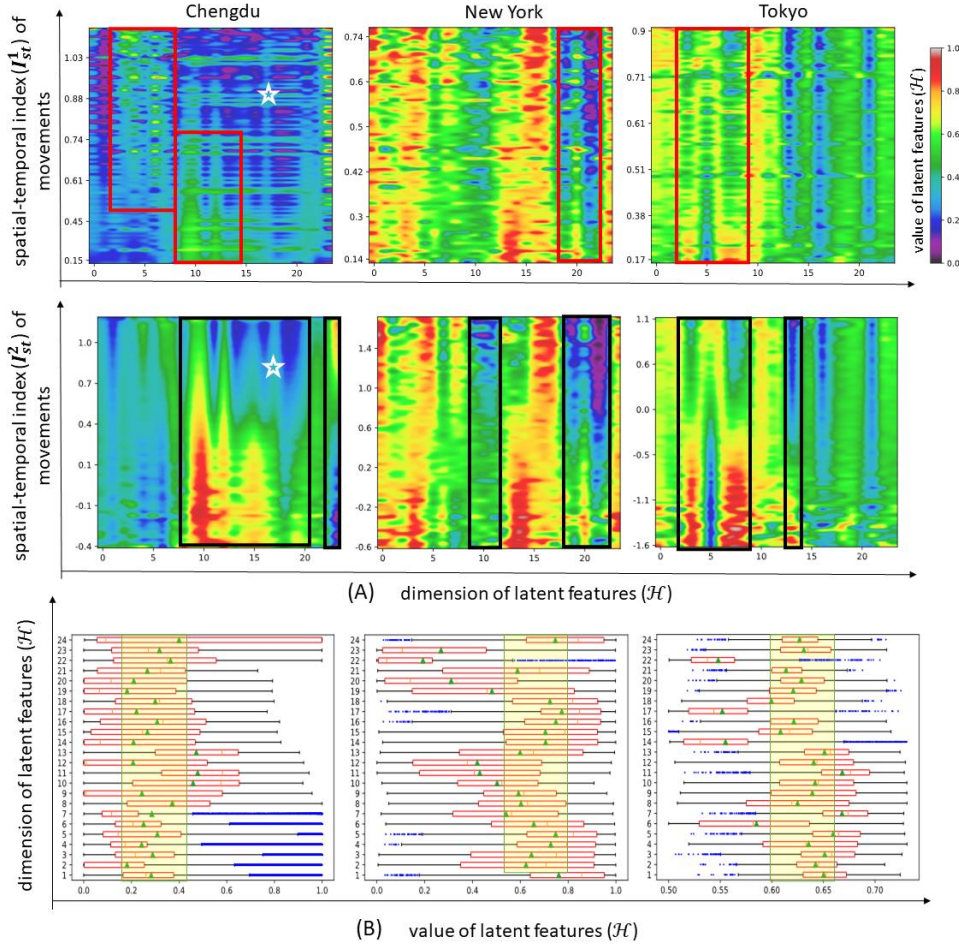


**Figure 7.** Spatial-temporal patterns represented in latent space. (A) refers to heat maps of neuronal response to spatial-temporal patterns; (B) refers to the statistical distribution of feature value of individual trajectory representations in latent space.

As shown in Figure 7-(A)-Chengdu, strong/weak response zones with distinct boundaries are formed in the latent feature space, and the response strength varies linearly in a specific range of dimensions. Detailly, in dimensions 2-7, we observed that the response intensified with the increasing  $I_{st}^1$ ; conersely, in dimensions 7-14, responses weakened with higher values of  $I_{st}^1$ . Showing that the neuronal responses in the two spans have a positive/negative linear relationship with the change of the spatial-temporal pattern defined by  $I_{st}^1$ . Notably, the responses to the pattern described by  $I_{st}^2$  is stronger and more pronounced. In dimensions 7-20, it is noted a reduction in neuronal responses as  $I_{st}^2$  increased, while in dimensions 22-24, the response strengthened with increased  $I_{st}^2$ . It is found that activated dimensional spans to  $I_{st}^1$  and  $I_{st}^2$  are partially similar, while the strength of their responses is differed significantly, especially in the regions around with the white star. This indicates that there are specified responses to space and time, and different compositions of these responses can represent different kinds of spatial-

temporal patterns. For instance, when the target pattern changes from  $I_{st}^1$  to  $I_{st}^2$ , there is observed a shift in the strong response interval from dimensions 2-14 to dimensions 7-20. This suggests that latent representations of ST-GraphRL adapt and represent different spatial-temporal patterns in a structured manner. On the New York and Tokyo datasets, where neurons were generally in a high activation, responses to specific spatial-temporal patterns were not much easy to bind, but some regularities in these responses can still be detected. In the New York dataset, there are similar negative linear responses to both  $I_{st}^1$  and  $I_{st}^2$ , while the  $I_{st}^2$ 's response is clearer and more continuous; moreover, a new response slightly emerges in dimensions 9-11 in  $I_{st}^2$ . In the Tokyo, the positive and negative response patterns were shown in  $I_{st}^1$  and  $I_{st}^2$  in dimension-9, respectively. And a significant negative linear response to  $I_{st}^2$  appeared in dimension-14. By analysing responses heat maps in all three datasets, it confirms that features learned in latent space enable to capture different spatial-temporal interactions by producing and compositing the corresponding responses.

We visualized the statistical information of representations to further study the reasons for the diverse response heat maps presented on the three datasets, which have uneven data size and individuals in them may have different moving patterns. The boxplot in Figure 7-(B) presents the distribution of the feature values of representations in 24 dimensions. It is found that the distributions in New York and Tokyo are similar, their outliers are dispersed, indicating that the neurons would be more active while less responsible for a certain response so that the representation is less sensitive to capture spatial-temporal patterns. In contrast, the feature values of the Chengdu dataset are polarized while tightly distributed, e.g., the outliers are concentrated in dimensions 1-7. Additionally, the span of distribution mean, marked with green triangles, in New York and Tokyo is concentrated at 0.5-0.8 and 0.6-0.66, respectively, while that of Chengdu is around 0.1-0.3; callback to Figure 7-(A), the dimensions whose mean value deviating from this span would be activated and responds to designated spatial-temporal patterns. It indicates that the larger training dataset helps ST-GraphRL to converge in a narrower latent space with a more compact feature distribution (Chung et al., 2022), as well as showing weaker neuronal sensitivity, i.e., only a small number of neurons would be activated when exposed to a specific spatial-temporal pattern, which is consistent with the response pattern of neurons in the human brain.

In summary, the linear response presented in latent space implies that the spatial-

temporal patterns can be explicitly observed and represented in the representation vectors generated by ST-GraphRL; in other words, ST-GraphRL successfully learns spatial-temporal interactions in ST-Graph and extracts patterns from these interaction features.

## 7. Conclusions

Spatial-temporal dependency is crucial for comprehending geospatial phenomena, making it essential for advancing the development of human-centric GeoFMs. However, the sparsity and high-dimensional coupling of spatial-temporal features within individual trajectories pose challenges in obtaining general-purpose trajectory representations capturing the spatial-temporal dependencies. To address this, this paper proposes a spatial-temporal joint representation learning method for individual trajectories. Experimental results on three real-world mobility datasets and investigation in the latent feature space validate the effectiveness of ST-GraphRL. Representations generated by ST-GraphRL were evaluated using multiple metrics, whose advantage is seen in its precise prediction of spatial-temporal movement distribution and accurate measurement of trajectory similarity, a task that other comparison approaches find challenging. It is attributed to two novel designs: (i) the spatial-temporal trajectory graph employs the temporal transition vector as a directed bridge linking spatial features. The explicit and structured display of space and time information can be used to record spatial-temporal interactions in movements; (ii) the two-stage jointly encoding model, including decoupling and fusing: independently encoding to establish initial embeddings of time and space aids in disentangling intricate spatial-temporal interactions; then message passing and aggregating operations joint space and time features promotes ST-GraphRL to effectively capture spatial-temporal dependencies. Furthermore, the decoder, promoting latent representations to statistically simulate spatial-temporal distributions of mobilities, aids in understanding mobility patterns.

The proposed representation learning method may also have implications for representation learnings of other geospatial data. In this particular instance, the spatial-temporal dependence of human mobility could be considered. This implication is particularly crucial for the advancement of GeoFMs, as their effectiveness may rely significantly on their ability to acquire Geo-knowledge and identify patterns concealed within various geospatial data sources.

## Reference

- Barbosa, H., Barthelemy, M., Ghoshal, G., James, C. R., Lenormand, M., Louail, T., Menezes, R., Ramasco, J. J., Simini, F., & Tomasini, M. (2018). Human mobility: Models and applications. *Physics Reports*, 734, 1–74. <https://doi.org/10.1016/j.physrep.2018.01.001>
- Bengio, Y., Courville, A., & Vincent, P. (2013). Representation Learning: A Review and New Perspectives. *IEEE Transactions on Pattern Analysis and Machine Intelligence*, 35(8), 1798–1828. <https://doi.org/10.1109/TPAMI.2013.50>
- Bommasani, R., Hudson, D. A., Adeli, E., Altman, R., Arora, S., von Arx, S., Bernstein, M. S., Bohg, J., Bosselut, A., Brunskill, E., Brynjolfsson, E., Buch, S., Card, D., Castellon, R., Chatterji, N., Chen, A., Creel, K., Davis, J. Q., Demszky, D., ... Liang, P. (2022). *On the Opportunities and Risks of Foundation Models* (arXiv:2108.07258). arXiv. <https://doi.org/10.48550/arXiv.2108.07258>
- Caron, M., Misra, I., Mairal, J., Goyal, P., Bojanowski, P., & Joulin, A. (2020). Unsupervised learning of visual features by contrasting cluster assignments. *Proceedings of the 34th International Conference on Neural Information Processing Systems*, 9912–9924.
- Chen, Y., Li, X., Cong, G., Bao, Z., Long, C., Liu, Y., Chandran, A. K., & Ellison, R. (2021). Robust Road Network Representation Learning: When Traffic Patterns Meet Traveling Semantics. *Proceedings of the 30th ACM International Conference on Information & Knowledge Management*, 211–220. <https://doi.org/10.1145/3459637.3482293>
- Chung, H. W., Hou, L., Longpre, S., Zoph, B., Tay, Y., Fedus, W., Li, Y., Wang, X., Dehghani, M., Brahma, S., Webson, A., Gu, S. S., Dai, Z., Suzgun, M., Chen, X., Chowdhery, A., Castro-Ros, A., Pellat, M., Robinson, K., ... Wei, J. (2022). *Scaling Instruction-Finetuned Language Models* (arXiv:2210.11416). arXiv. <https://doi.org/10.48550/arXiv.2210.11416>
- Damiani, M. L., Acquaviva, A., Hachem, F., & Rossini, M. (2020). Learning Behavioral Representations of Human Mobility. *Proceedings of the 28th International Conference on Advances in Geographic Information Systems*, 367–376. <https://doi.org/10.1145/3397536.3422255>
- Damiani, M. L., Hachem, F., Quadri, C., & Gaito, S. (2019). Location relevance and diversity in symbolic trajectories with application to telco data. *Proceedings of the 16th International Symposium on Spatial and Temporal Databases*, 41–50. <https://doi.org/10.1145/3340964.3340980>
- Devlin, J., Chang, M.-W., Lee, K., & Toutanova, K. (2019). BERT: Pre-training of Deep Bidirectional Transformers for Language Understanding. In J. Burstein, C. Doran, & T. Solorio (Eds.), *Proceedings of the 2019 Conference of the North American Chapter of the Association for Computational Linguistics: Human Language Technologies, Volume 1 (Long and Short Papers)* (pp. 4171–4186). Association for Computational Linguistics. <https://doi.org/10.18653/v1/N19-1423>
- Ericsson, L., Gouk, H., Loy, C. C., & Hospedales, T. M. (2022). Self-Supervised Representation Learning: Introduction, advances, and challenges. *IEEE Signal Processing Magazine*, 39(3), 42–62. <https://doi.org/10.1109/MSP.2021.3134634>
- Gao, Q., Zhou, F., Zhang, K., Trajcevski, G., Luo, X., & Zhang, F. (2017). Identifying human mobility via trajectory embeddings. *Proceedings of the 26th International Joint Conference on Artificial Intelligence*, 1689–1695.
- Gao, Q., Zhou, F., Zhong, T., Trajcevski, G., Yang, X., & Li, T. (2022). Contextual spatio-temporal graph representation learning for reinforced human mobility mining. *Information Sciences*, 606, 230–249. <https://doi.org/10.1016/j.ins.2022.05.049>
- Glake, D., Panse, F., Lenfers, U., Clemen, T., & Ritter, N. (2022). Spatio-temporal Trajectory Learning using Simulation Systems. *Proceedings of the 31st ACM International Conference on Information & Knowledge Management*, 592–602. <https://doi.org/10.1145/3511808.3557457>
- Grill, J.-B., Strub, F., Altché, F., Tallec, C., Richemond, P. H., Buchatskaya, E., Doersch, C., Pires, B. A., Guo, Z. D., Azar, M. G., Piot, B., Kavukcuoglu, K., Munos, R., & Valko, M. (2020). *Bootstrap your own latent: A new approach to self-supervised Learning* (arXiv:2006.07733). arXiv. <https://doi.org/10.48550/arXiv.2006.07733>
- Hu, S., Gao, S., Luo, W., Wu, L., Li, T., Xu, Y., & Zhang, Z. (2023). Revealing intra-urban hierarchical spatial structure through representation learning by combining road network abstraction model and taxi trajectory data. *Annals of GIS*, 0(0), 1–18. <https://doi.org/10.1080/19475683.2023.2241526>
- Janowicz, K., Gao, S., McKenzie, G., Hu, Y., & Bhaduri, B. (2020). GeoAI: Spatially explicit artificial intelligence techniques for geographic knowledge discovery and beyond. *International Journal of*



- Geographical Information Science*, 34(4), 625–636.  
<https://doi.org/10.1080/13658816.2019.1684500>
- Jiang, J., Pan, D., Ren, H., Jiang, X., Li, C., & Wang, J. (2022). *Self-supervised Trajectory Representation Learning with Temporal Regularities and Travel Semantics* (arXiv:2211.09510). arXiv. <https://doi.org/10.48550/arXiv.2211.09510>
- Kong, D., & Wu, F. (2018). HST-LSTM: A Hierarchical Spatial-Temporal Long-Short Term Memory Network for Location Prediction. *Proceedings of the Twenty-Seventh International Joint Conference on Artificial Intelligence*, 2341–2347. <https://doi.org/10.24963/ijcai.2018/324>
- Li, G., Xiong, C., Thabet, A., & Ghanem, B. (2020). *DeeperGCN: All You Need to Train Deeper GCNs* (arXiv:2006.07739). arXiv. <https://doi.org/10.48550/arXiv.2006.07739>
- Li, M., Gao, S., Lu, F., Liu, K., Zhang, H., & Tu, W. (2021). Prediction of human activity intensity using the interactions in physical and social spaces through graph convolutional networks. *International Journal of Geographical Information Science*, 35(12), 2489–2516. <https://doi.org/10.1080/13658816.2021.1912347>
- Li, X., Zhao, K., Cong, G., Jensen, C. S., & Wei, W. (2018). Deep Representation Learning for Trajectory Similarity Computation. *IEEE International Conference on Data Engineering*, 617–628. <https://doi.org/10.1109/icde.2018.00062>
- Liu, J., Chen, Y., Huang, X., Li, J., & Min, G. (2023). GNN-based long and short term preference modeling for next-location prediction. *Information Sciences*, 629, 1–14. <https://doi.org/10.1016/j.ins.2023.01.131>
- Liu, X., Wu, M., Peng, B., & Huang, Q. (2022). Graph-based representation for identifying individual travel activities with spatiotemporal trajectories and POI data. *Scientific Reports*, 12(1), 15769. <https://doi.org/10.1038/s41598-022-19441-9>
- Mai, G., Huang, W., Sun, J., Song, S., Mishra, D., Liu, N., Gao, S., Liu, T., Cong, G., Hu, Y., Cundy, C., Li, Z., Zhu, R., & Lao, N. (2023). *On the Opportunities and Challenges of Foundation Models for Geospatial Artificial Intelligence* (arXiv:2304.06798). arXiv. <https://doi.org/10.48550/arXiv.2304.06798>
- Martin, H., Bucher, D., Suel, E., Zhao, P., Perez-Cruz, F., & Raubal, M. (2023). *Graph Convolutional Neural Networks for Human Activity Purpose Imputation from GPS-based Trajectory Data*. <https://openreview.net/forum?id=H1xYUOmy1V>
- Ordóñez Medina, S. A. (2018). Inferring weekly primary activity patterns using public transport smart card data and a household travel survey. *Travel Behaviour and Society*, 12, 93–101. <https://doi.org/10.1016/j.tbs.2016.11.005>
- Scheider, S., & Richter, K.-F. (2023). GeoAI. *KI - Künstliche Intelligenz*, 37(1), 5–9. <https://doi.org/10.1007/s13218-022-00797-z>
- Tao, C., Yang, Z., & Haworth, J. (2022). Network and graph-based SpaceTimeAI: Conception, method and applications. *Acta Geodaetica et Cartographica Sinica*, 51(7), 1629. <https://doi.org/10.11947/j.AGCS.2022.20220236>
- Vaswani, A., Shazeer, N., Parmar, N., Uszkoreit, J., Jones, L., Gomez, A. N., Kaiser, Ł., & Polosukhin, I. (2017). Attention is All you Need. *Advances in Neural Information Processing Systems*, 30. [https://proceedings.neurips.cc/paper\\_files/paper/2017/hash/3f5ee243547dee91fbd053c1c4a845aa-Abstract.html](https://proceedings.neurips.cc/paper_files/paper/2017/hash/3f5ee243547dee91fbd053c1c4a845aa-Abstract.html)
- Vaswani, A., Shazeer, N., Parmar, N., Uszkoreit, J., Jones, L., Gomez, A. N., Kaiser, L., & Polosukhin, I. (2023). *Attention Is All You Need* (arXiv:1706.03762). arXiv. <https://doi.org/10.48550/arXiv.1706.03762>
- Veličković, P., Cucurull, G., Casanova, A., Romero, A., Liò, P., & Bengio, Y. (2018). *Graph Attention Networks* (arXiv:1710.10903). arXiv. <http://arxiv.org/abs/1710.10903>
- Veličković, P., Fedus, W., Hamilton, W. L., Liò, P., Bengio, Y., & Hjelm, R. D. (2018). *Deep Graph Infomax* (arXiv:1809.10341). arXiv. <http://arxiv.org/abs/1809.10341>
- Wang, D., Wang, P., Liu, K., Zhou, Y., Hughes, C. E., & Fu, Y. (2021). Reinforced Imitative Graph Representation Learning for Mobile User Profiling: An Adversarial Training Perspective. *Proceedings of the AAAI Conference on Artificial Intelligence*, 35(5), Article 5. <https://doi.org/10.1609/aaai.v35i5.16567>
- Wang, P., Fu, Y., Xiong, H., & Li, X. (2019). Adversarial Substructured Representation Learning for Mobile User Profiling. *Proceedings of the 25th ACM SIGKDD International Conference on Knowledge Discovery & Data Mining*, 130–138. <https://doi.org/10.1145/3292500.3330869>

- Wu, T., Huang, Q., Liu, Z., Wang, Y., & Lin, D. (2021). *Distribution-Balanced Loss for Multi-Label Classification in Long-Tailed Datasets* (arXiv:2007.09654). arXiv. <https://doi.org/10.48550/arXiv.2007.09654>
- Xu, X. (2021). Context-based Trajectory Prediction with LSTM Networks. *Proceedings of the 2020 3rd International Conference on Computational Intelligence and Intelligent Systems*, 100–104. <https://doi.org/10.1145/3440840.3440842>
- Yang, D., Zhang, D., Zheng, V. W., & Yu, Z. (2015). Modeling User Activity Preference by Leveraging User Spatial Temporal Characteristics in LBSNs. *IEEE Transactions on Systems, Man, and Cybernetics: Systems*, 45(1), 129–142. <https://doi.org/10.1109/TSMC.2014.2327053>
- Yang, S. B., Guo, C., Hu, J., Tang, J., & Yang, B. (2021). Unsupervised Path Representation Learning with Curriculum Negative Sampling. *Proceedings of the Thirtieth International Joint Conference on Artificial Intelligence*, 3286–3292. <https://doi.org/10.24963/ijcai.2021/452>
- Yu, W., & Wang, G. (2023). Graph based embedding learning of trajectory data for transportation mode recognition by fusing sequence and dependency relations. *International Journal of Geographical Information Science*, 1–24. <https://doi.org/10.1080/13658816.2023.2268668>
- Zhang, Y., Cheng, T., Ren, Y., & Xie, K. (2020). A novel residual graph convolution deep learning model for short-term network-based traffic forecasting. *International Journal of Geographical Information Science*, 34(5), 969–995. <https://doi.org/10.1080/13658816.2019.1697879>
- Zhang, Y., Wei, C., Wu, S., He, Z., & Yu, W. (2023, July 16). *GeoGPT: Understanding and Processing Geospatial Tasks through An Autonomous GPT*. arXiv.Org. <https://arxiv.org/abs/2307.07930v1>
- Zhang, Y., Zhao, T., Gao, S., & Raubal, M. (2023). Incorporating multimodal context information into traffic speed forecasting through graph deep learning. *International Journal of Geographical Information Science*, 37(9), 1909–1935. <https://doi.org/10.1080/13658816.2023.2234959>
- Zhou, J., Cui, G., Hu, S., Zhang, Z., Yang, C., Liu, Z., Wang, L., Li, C., & Sun, M. (2020). Graph neural networks: A review of methods and applications. *AI Open*, 1, 57–81. <https://doi.org/10.1016/j.aiopen.2021.01.001>